

Letter to editor

Gold-bearing ferroselite (FeSe₂) from Trogtal, Harz, Germany, and significance of its Co/Ni ratio

Alexandre Raphael CABRAL^{1*}, Nikola KOGLIN², Helene BRÄTZ³¹ Mineral Deposits, Technische Universität Clausthal, Adolph-Roemer-Str. 2A, 38678 Clausthal-Zellerfeld, Germany; alexandre.cabral@tu-clausthal.de² Geodynamics and Geomaterials Research Division, Universität Würzburg, Am Hubland, 97074 Würzburg, Germany³ GeoZentrum Nordbayern, Lithosphere Dynamics, Schloßgarten 5a, 91054 Erlangen, Germany

* Corresponding author



Ferroselite from Trogtal, the type locality of the cobalt selenide trogtalite, in the Harz Mountains, Germany, forms a trogtalite–ferroselite assemblage in pockets of massive clausenthalite in which specular hematite is dispersed. The pockets occur in hematite-impregnated carbonate veins, emplaced in a reddened greywacke of Lower Carboniferous age. Ferroselite contains ~0.2–5.0 ppm Au; trogtalite has even higher Au contents. Ferroselite has Co/Ni ratios mostly above unity. These characteristics likely reflect oxidizing brines with Co/Ni > 1, such as those involved in the formation of sediment-hosted copper deposits.

Keywords: ferroselite, trogtalite, Co/Ni ratio, Trogtal, Harz, Germany

Received: 9 October 2012; **accepted:** 3 January 2013; **handling editor:** F. Laufek

1. Introduction

Numerous studies have been concerned with the content and distribution of Au in sulfide minerals, particularly in pyrite and arsenopyrite (e.g., Benzaouza et al. 2007; Wagner et al. 2007; Cook et al. 2009; Koglin et al. 2010; Majzlan et al. 2010; Thomas et al. 2011). Pyrite has also been investigated for other trace and minor elements. Among them, the contents of Co and Ni in pyrite, specifically its Co/Ni ratios, have been used as an indicator of the environment of pyrite formation (e.g., Loftus-Hills and Solomon 1967; Bralía et al. 1979; Clark et al. 2004; Marques et al. 2006; Koglin et al. 2010; Pal et al. 2011). Recently, the Co/Ni ratio in arsenopyrite has been applied to constrain the fluid source for an Au-lode deposit (Cabral and Koglin 2012).

Compared to pyrite and other sulfide minerals, little information on the trace contents of Au and Co/Ni ratios in selenide minerals is available. Can ferroselite, the Se analogue of pyrite, host trace contents of Au? Can the Co/Ni ratio in a Fe selenide hint at the fluid chemistry and/or fluid provenance of a selenide vein-type deposit? Here we provide evidence that ferroselite, FeSe₂, from Trogtal (Harz Mountains, Germany) contains trace amounts of Au. We also discuss the genetic significance of the Co/Ni ratio in this ferroselite.

2. Trogtal and selenide-bearing veins

Trogtal is a small tributary valley near Lautenthal, in the north-western Harz Mountains. A quarry in the Trogtal

exploited greywacke that hosted selenide minerals. A Lower Carboniferous age for the greywacke is ascertained by abundant fossils of *Goniatites*, *striatus* zone (Figge 1964). The selenide minerals were found in veins, up to 3 cm thick, in the greywacke (Frebold 1927b; Tischendorf 1959). The veins consist of several generations of carbonate, with, or without, red pigmentation by fine-grained specular hematite. Such a red pigmentation also characterizes the greywacke host rock. The main selenide mineral identified is clausenthalite, PbSe, which sporadically fills interstitial spaces within the vein-carbonate aggregates. Frebold (1927a) recognized that grains of cobaltite, i.e., “Kobaltglanz”, are intensively corroded by clausenthalite. He also noted that specular hematite is intergrown with cobaltite. The identification as cobaltite was later refuted by Ramdohr (1928), who suggested the possible occurrence of at least four different selenides of Co. These were subsequently characterized as trogtalite, cubic CoSe₂, “hastite”, asserted as orthorhombic CoSe₂, bornhardite, cubic Co₃Se₄, and freboldite, hexagonal CoSe (Ramdohr and Schmitt 1955). The mineral “hastite” has recently been discredited as being identical with ferroselite, orthorhombic FeSe₂ (Keutsch et al. 2009).

3. Samples and experimental methods

Polished sections labeled ‘Trogtal’ were found, together with an offprint of Ramdohr and Schmitt’s (1955) article, in the collection of late Professor Krause (1925–2010) at

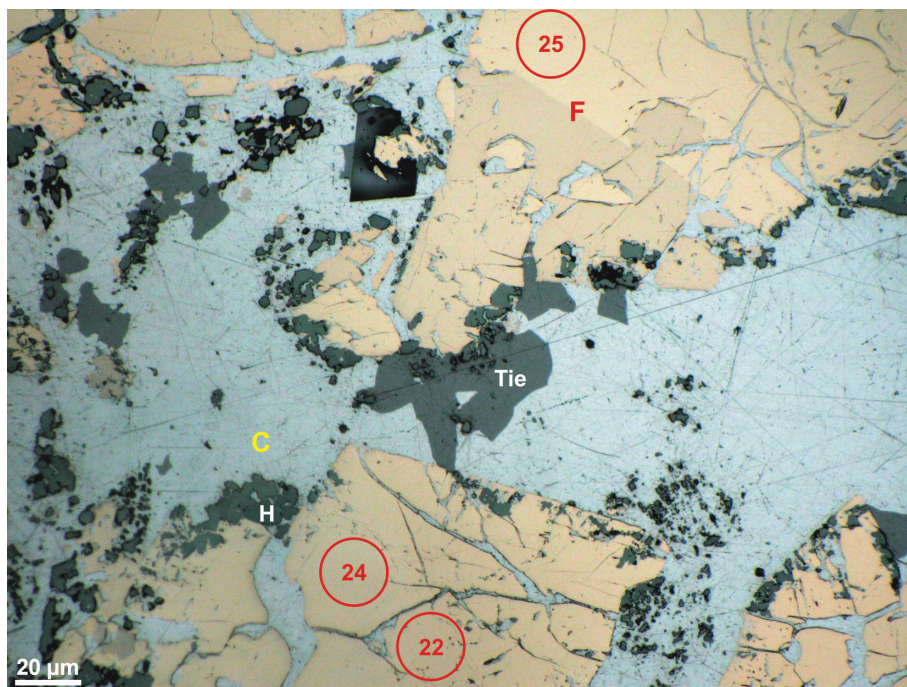


Fig. 1 Reflected-light photomicrograph (oil immersion) of ferroselite from Trogtal, Harz, Germany. The ferroselite (F, shades of pale yellow) occurs in a matrix of clausthalite (C, bluish white), which contains hematite (H, grey) and tiemannite (Tie, grey but softer than hematite). The ferroselite has cracks that are filled with clausthalite. Circles are LA-ICP-MS spots and their numbers correspond to those of analyses in Tab. 2.

Technische Universität Clausthal. The name ‘Schell’ was additionally written on two of the four polished sections. Ramdohr and Schmitt (1955) acknowledged an old miner of the Trogtal quarry, Schell, for having provided them with some selenide-bearing samples in which the aforementioned selenides of Co were characterized. Hence, the samples studied here come from the type locality of trogtalite.

Ferroselite and trogtalite had their chemical compositions determined by wavelength-dispersion analysis using a Cameca SX 100 electron microprobe at Technische Universität Clausthal. The analyses were performed at 20 kV and 20 nA, with beam size of 1 and 10 μm . The following reference materials and X-ray lines were employed: pure metals (SeL_α , FeK_α , CoK_α , NiK_α , CuK_α), PbTe (PbM_α) and FeS_2 (SK_α).

After the reconnaissance electron-microprobe work (Tab. 1), trace elements in the selenides were determined by laser ablation-inductively coupled plasma-mass spectrometry (LA-ICP-MS) at GeoZentrum Nordbayern, Universität Erlangen. The instrument is an Agilent 7500i ICP-MS, coupled to an UP193FX, New Wave Research Excimer Laser, which was operated using plasma power of 1320 W, carrier gas I (He) at 0.65 l/min, carrier gas II (Ar) at 1.10 l/min, plasma gas (Ar) at 14.9 l/min and auxiliary gas (Ar) at 0.9 l/min. The analytical conditions of the instrument were as follows: single spot of 20 μm , repetition rate of 20 Hz, irradiance of 0.58 GW/cm^2 , fluence of 2.9 J/cm^2 , 20 s for background and 25 s for sample measurements in time-resolved analytical mode at maximum peak. The isotopes analysed for were: ^{77}Se at 1-ms integration

time; ^{29}Si and ^{59}Co at 5-ms integration time; ^{33}S , ^{34}S , ^{63}Cu , ^{65}Cu and ^{57}Fe at 10-ms integration time; ^{55}Mn , ^{60}Ni , ^{66}Zn , ^{71}Ga , ^{75}As , ^{95}Mo , ^{99}Ru , ^{101}Ru , ^{103}Rh , ^{105}Pd , ^{108}Pd , ^{109}Ag , ^{111}Cd , ^{115}In , ^{118}Sn , ^{121}Sb , ^{125}Te , ^{185}Re , ^{189}Os , ^{193}Ir , ^{195}Pt , ^{197}Au , ^{202}Hg , ^{205}Tl , ^{208}Pb and ^{209}Bi at 30-ms integration time. The content of Fe that had been determined by the electron microprobe was used for internal standardization. Reference materials for external calibration were Po724 B2 of the Memorial University of Newfoundland (Ru, Rh, Pd, Os, Ir, Pt and Au), (Fe, Ni) $_{1-x}\text{S}$ for Ni and Re (Wohlgemuth-Ueberwasser et al. 2007) and MASS-1 polymetal sulfide of the United States Geological Survey (S, Mn, Co, Cu, Zn, Ga, As, Se, Mo, Ag, Cd, In, Sn, Sb, Te, Hg, Tl, Pb and Bi). The LA-ICP-MS measurements were evaluated off-line by means of GLITTER (van Achterbergh et al. 2000). Concentrations are given in parts per million (ppm) in Tab. 2, together with detection limits, precision and accuracy.

4. Results

Ferroselite occurs as grains that are commonly less than 100 μm in length, enclosed in clausthalite (Fig. 1). The grains contain cracks filled with clausthalite. Specular hematite and subordinate tiemannite, HgSe, are present on the surface of ferroselite, in interstices between ferroselite grains (Fig. 1), and in clausthalite-filled cracks within ferroselite (Fig. 2). Contrary to ferroselite, which does not show obvious signs of replacement, early trogtalite is extensively replaced by clausthalite. A late generation of trogtalite overgrows the corroded trogtalite,

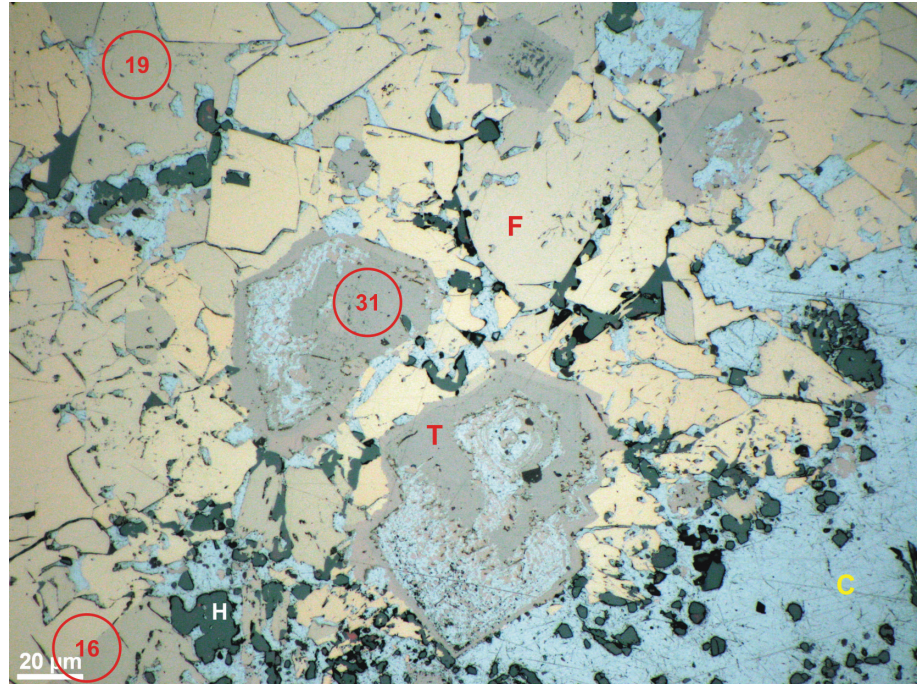


Fig. 2 Reflected-light photomicrograph (oil immersion) of ferroselite–trogtalite aggregates from Trogtal, Harz, Germany. The trogtalite (T, shades of pale brown) is corroded and partially replaced by clausenthalite (C, bluish white). The ferroselite (F, shades of pale yellow) has sharp contacts with a late generation of trogtalite, which forms a rim around the corroded trogtalite (i.e., atoll-like microstructure). Hematite (H) appears as greyish platelets. Circles are LA–ICP–MS spots and their numbers correspond to those of analyses in Tab. 2.

forming a rim that composes an atoll-like microstructure (Fig. 2). This rim of late trogtalite has sharp, essentially rectilinear contacts with the immediately adjacent ferroselite. The late trogtalite also occurs as independent grains not altered by clausenthalite.

The electron-microprobe analyses indicate that the Trogtal ferroselite corresponds to nearly stoichiometric FeSe_2 ; however, a few microanalyses give Pb in the range of a few weight per cent, up to 2.4 wt. % (Tab. 1). In contrast to ferroselite, the early and late generations

of trogtalite diverge from the end-member composition. The trogtalite contains variable amounts of Co, Ni and Cu, with the late generation having more Co and less Cu than the early trogtalite. Overall, the results of the electron-microprobe work agree with the compositional data reported in Keutsch et al. (2009).

The LA–ICP–MS measurements show that ferroselite contains traces of Au and Ag, ~0.2–5.0 ppm and ~4.0–38 ppm, respectively (Tab. 2). However, Pb concentrations obtained in ferroselite, up to ~25 wt. % Pb, relate to

Tab. 1 Results of electron-microprobe analyses of ferroselite and trogtalite from Trogtal, Harz, Germany

| Analysis number | 1 | 2 | 3 | 4 | 5 | 6 | 7 | 8 | 9 | 10 | 11 | 12 | 13* | 14 | 15 |
|-----------------|--------|--------|--------|-------|-------|-------|-------|-------|--------|-------|--------|-------|-------|--------|--------|
| S (wt. %) | <0.05 | <0.05 | <0.05 | <0.05 | <0.05 | <0.06 | <0.05 | <0.05 | <0.05 | <0.05 | <0.05 | <0.06 | 0.14 | 0.11 | 0.13 |
| Fe | 26.46 | 26.35 | 26.40 | 26.33 | 26.30 | 26.46 | 26.37 | 26.48 | 26.51 | 26.18 | 25.78 | 0.23 | 0.67 | 0.67 | 0.77 |
| Co | <0.06 | <0.06 | 0.07 | <0.06 | <0.05 | 0.11 | <0.06 | <0.06 | <0.06 | <0.06 | <0.05 | 14.48 | 22.31 | 22.66 | 23.02 |
| Ni | <0.06 | <0.06 | <0.06 | <0.06 | <0.06 | <0.06 | <0.06 | <0.06 | <0.06 | <0.06 | <0.06 | 5.11 | 3.48 | 3.31 | 3.83 |
| Cu | <0.12 | <0.13 | <0.12 | <0.13 | <0.13 | <0.12 | <0.13 | <0.14 | <0.13 | <0.13 | <0.12 | 7.65 | 1.05 | 0.84 | 0.25 |
| Se | 73.75 | 72.90 | 73.70 | 72.98 | 73.52 | 73.17 | 73.33 | 73.31 | 73.73 | 73.46 | 72.50 | 71.92 | 72.32 | 72.73 | 72.62 |
| Pb | <0.60 | 1.19 | <0.60 | <0.60 | <0.60 | <0.60 | <0.60 | <0.60 | <0.60 | <0.60 | 2.39 | <0.60 | n.a. | n.a. | n.a. |
| Total | 100.20 | 100.44 | 100.16 | 99.30 | 99.82 | 99.75 | 99.70 | 99.79 | 100.24 | 99.64 | 100.67 | 99.40 | 99.96 | 100.32 | 100.63 |
| Apfu | | | | | | | | | | | | | | | |
| S | | | | | | | | | | | | | 0.01 | 0.01 | 0.01 |
| Se | 1.99 | 1.98 | 1.99 | 1.99 | 1.99 | 1.98 | 1.99 | 1.99 | 1.99 | 1.99 | 1.98 | 2.00 | 1.98 | 1.99 | 1.97 |
| Fe | 1.01 | 1.01 | 1.01 | 1.01 | 1.01 | 1.01 | 1.01 | 1.01 | 1.01 | 1.01 | 1.00 | 0.01 | 0.03 | 0.03 | 0.03 |
| Co | | | | | | | | | | | | 0.54 | 0.82 | 0.83 | 0.84 |
| Ni | | | | | | | | | | | | 0.19 | 0.13 | 0.12 | 0.14 |
| Cu | | | | | | | | | | | | 0.26 | 0.04 | 0.03 | 0.01 |
| Pb | | 0.01 | | | | | | | | | 0.02 | | | | |

1–11: ferroselite, beam diameter of 10 µm; 12–15: trogtalite, beam diameter of 1 µm; early (12) and late (13*–15) trogtalite.

* Average values of six microanalyses on the same grain of trogtalite.

Apfu = atoms per formula unit on the basis of 3 atoms; n.a. = not analysed.

Tab. 2 Results of LA-ICP-MS analyses of ferroselite and trogtalite from Trogtal, Harz, Germany

| Analysis number | 16 | 17 | 18 | 19 | 20 | 21 | 22 | 23 | 24 | 25 | 26 | 27 | 28 | 29 | 30 | 31 | 32 | DL | RM |
|-----------------|-------|-------|-------|--------|-------|-------|--------|-------|-------|-------|--------|-------|--------|-------|-------|--------|--------|----------------|----------------|
| Tab. 1* | 1 | 2 | 4 | 5 | 7 | 8 | 9 | 10 | 11 | 12 | | | | | | | | | |
| S (ppm) | 1872 | 1719 | 1974 | 1080 | 2217 | 2493 | 1730 | 1527 | 1113 | 2089 | 2290 | 2219 | 1534 | 2662 | 2219 | 3617 | 734 | 403064 ± 13589 | |
| Mn | <0.3 | <0.3 | <0.3 | <0.3 | <0.3 | <0.2 | <0.2 | <0.2 | <0.3 | <0.3 | <0.3 | <0.3 | <0.3 | 0.5 | <0.4 | 0.3 | <0.4 | 0.5 | 286 ± 12 |
| Co | 236 | 59 | 33 | 427 | 93 | 174 | 144 | 84 | 128 | 507 | 139 | 86 | 62 | 85 | 28125 | 99777 | 224464 | 0.3 | 61 ± 3 |
| Ni | 88 | 32 | 22 | 292 | 55 | 220 | 109 | 102 | 81 | 36 | 49 | 64 | 20 | 92 | 11496 | 65015 | 48744 | 0.3 | 49263 ± 868 |
| Cu | 348 | 223 | 51 | 206 | 209 | 128 | 72 | 60 | 162 | 338 | 86 | 72 | 16 | 120 | 466 | 76204 | 2444 | 1.1 | 137128 ± 11795 |
| Zn | <1.5 | <1.3 | <1.6 | <1.4 | <1.5 | <1.5 | <1.6 | 1.4 | 1.6 | <1.4 | <1.8 | <1.5 | <1.4 | <1.3 | <2.1 | <0.6 | <2.1 | 1.4 | 216800 ± 11847 |
| Ga | <0.08 | <0.05 | <0.07 | <0.07 | <0.08 | <0.06 | <0.06 | <0.05 | <0.06 | <0.06 | <0.07 | <0.07 | <0.06 | <0.07 | <0.08 | <0.02 | <0.11 | 0.1 | 65 ± 2 |
| As | 13 | <0.3 | 1.1 | 1.3 | <0.4 | 2.5 | 2.9 | 1.1 | 1.1 | 2.2 | 1.3 | 1.5 | 3.2 | 1.2 | 11 | 6.7 | 94 | 0.3 | 66 ± 2 |
| Mo | <0.14 | <0.15 | <0.10 | 0.26 | <0.15 | <0.16 | <0.15 | 0.19 | 0.21 | 0.21 | 0.17 | 0.20 | <0.11 | 0.15 | <0.17 | <0.12 | 0.25 | 0.2 | 59 ± 5 |
| Pd** | <0.07 | <0.05 | <0.07 | <0.08 | <0.07 | <0.07 | <0.08 | <0.04 | <0.04 | <0.06 | <0.06 | 0.10 | <0.06 | <0.07 | <0.10 | 0.25 | 0.46 | 0.07 | 45.8 ± 1.7 |
| Ag | 17 | 4.3 | 6.6 | 17 | 6.3 | 21 | 27 | 5.8 | 11 | 13 | 38 | 20 | 10 | 19 | 26 | 124 | 47 | 0.05 | 51 ± 3 |
| Cd | <0.3 | <0.3 | <0.4 | 1.3 | 0.9 | 4.1 | 1.2 | 0.4 | 3.3 | 0.5 | 0.5 | 9.4 | <0.4 | <0.3 | 1.5 | 13 | 0.8 | 0.3 | 65 ± 10 |
| In | <0.02 | <0.01 | <0.02 | <0.02 | <0.01 | <0.02 | <0.01 | <0.01 | <0.01 | <0.02 | <0.02 | <0.02 | <0.01 | <0.01 | <0.02 | 0.02 | <0.02 | 0.02 | 52 ± 3 |
| Sn | 0.9 | 0.9 | 1.2 | 0.4 | 0.7 | 0.7 | 0.7 | 0.6 | 0.8 | 0.5 | 0.5 | 0.9 | 0.8 | 1.0 | 1.3 | 0.4 | 1.2 | 0.2 | 60 ± 2 |
| Sb | 19 | 2.7 | 3.5 | 24 | 9.1 | 13 | 30 | 6.3 | 12 | 14 | 27 | 19 | 15 | 5.0 | 23 | 35 | 37 | 0.09 | 61 ± 2 |
| Te | 87 | 98 | 35 | 31 | 43 | 87 | 47 | 31 | 85 | 37 | 75 | 67 | 8.3 | 8.9 | 122 | 145 | 474 | 0.5 | 15 ± 1 |
| Re | <0.05 | <0.07 | <0.05 | <0.08 | <0.07 | <0.08 | <0.06 | <0.05 | <0.05 | <0.06 | 0.09 | <0.04 | <0.06 | <0.05 | <0.11 | <0.05 | 0.11 | 0.09 | 14.7 ± 1.9 |
| Os | <0.15 | <0.14 | <0.17 | <0.17 | <0.19 | <0.19 | <0.12 | <0.12 | <0.08 | 0.20 | <0.15 | <0.16 | <0.14 | <0.15 | <0.24 | 0.21 | 0.24 | 0.2 | 36.0 ± 1.3 |
| Ir | <0.04 | <0.04 | <0.04 | <0.04 | <0.06 | <0.04 | <0.04 | <0.04 | 0.04 | <0.04 | <0.04 | <0.04 | <0.04 | <0.03 | 0.08 | <0.03 | <0.06 | 0.04 | 37.4 ± 1.5 |
| Pt | <0.09 | <0.08 | <0.04 | <0.09 | <0.08 | <0.08 | 0.18 | <0.08 | 0.06 | <0.08 | <0.08 | 0.08 | <0.07 | <0.08 | <0.14 | 0.59 | 1.2 | 0.08 | 36.1 ± 1.3 |
| Au | 2.4 | 0.61 | 0.32 | 2.0 | 0.24 | 2.1 | 2.3 | 0.69 | 1.7 | 1.4 | 0.84 | 1.5 | 0.51 | 0.51 | 5.1 | 6.6 | 9.5 | 0.06 | 45.0 ± 4.7 |
| Hg | 673 | 136 | 123 | 945 | 39 | 2624 | 1015 | 147 | 2066 | 424 | 203 | 2818 | 40 | 124 | 369 | 8251 | 180 | 0.5 | 51 ± 16 |
| Tl | 5.3 | 0.68 | 0.50 | 2.9 | 0.29 | 7.9 | 3.7 | 6.9 | 2.4 | 3.9 | 3.7 | 5.2 | 0.92 | 1.2 | 2.4 | 3.8 | 1.9 | 0.03 | 51 ± 2 |
| Pb*** | 79333 | 10073 | 9232 | 126452 | 69490 | 34753 | 190212 | 18706 | 16175 | 26747 | 252227 | 38493 | 138684 | 6931 | 55466 | 108201 | 101833 | 0.3 | 71 ± 5 |
| Bi | 3.1 | 0.65 | 0.95 | 10 | 5.7 | 2.6 | 13 | 2.7 | 1.3 | 2.0 | 15 | 6.5 | 2.7 | 0.42 | 3.1 | 40 | 8.8 | 0.04 | 62 ± 3 |
| Co/Ni | 2.7 | 1.8 | 1.5 | 1.5 | 1.7 | 0.8 | 1.3 | 0.8 | 1.6 | 14.1 | 2.8 | 1.3 | 3.1 | 0.9 | 2.4 | 1.5 | 4.6 | | |

16–30: ferroselite; 31–32: trogtalite.

DL: detection limit of the respective element.

RM: measurements on reference materials to determine precision and accuracy. For Ni and Re – (Fe,Ni)_{1-x}S_x; for Pd, Os, Ir, Pt and Au – Po724 B2; for all other elements – MASS-1.

* Numbers refer to the analysis number of electron-microprobe results reported in Tab. 1.

** Values for Pd are corrected for interference with ¹⁰⁸Cd.

*** Values for Pb reflect ablation of the enclosing clausenthalite and should thus be considered with caution.

Values for Ru and Rh are not reported due to interferences (e.g., ⁹⁹Ru = ⁵⁹Co⁴⁰Ar, ¹⁰³Rh = ²⁰⁶Pb³⁷).

the clausthalite matrix because the Pb signal invariably increased as the sample ablation proceeded, as observed in the time-resolved analytical mode. The highest values of Au, about 7 and 10 ppm, are measured in trogtalite. Considering all measurements, both on ferroselite and trogtalite, Au and Co are significantly positively correlated (Fig. 3a, with a squared correlation coefficient, r^2 , of 0.92), whereas Au shows no correlation with Pb (Fig. 3b). Trogtalite is also richer in Pt and Pd relative to ferroselite (~ 1.0 Pt and ~ 0.5 ppm Pd, Tab. 2).

The LA-ICP-MS results give a wide range of Co and Ni contents in ferroselite, from ~ 30 ppm to ~ 3.0 wt. % and from ~ 20 ppm to ~ 1.0 wt. %, respectively. In contrast, both elements are consistently low, mostly lower than 0.06 wt. %, in the electron-microprobe analyses (Tab. 1). Consequently, Co and Ni values above 0.06 wt. % are regarded as contamination from trogtalite, or other Co-rich minerals, during laser ablation. Most analyses of ferroselite have Co/Ni ratios that are above unity, even if those above 500 ppm Co are excluded. For those with < 500 ppm Co, ferroselite has Co/Ni ratios that extend from 0.8 to 3.1, averaging 1.7 ± 0.8 ($n = 13$, three of which have Co/Ni ratios below unity).

The Trogtal ferroselite contains an assemblage of trace elements that characterize deposits in the epithermal temperature range, such as Hg (up to ~ 2800 ppm) and Sb (up to 30 ppm), with ratios of Sb/As > 1 . The mineral also hosts trace contents of Te (up to 98 ppm) and Tl (up to 8 ppm).

5. Discussion

The Au enrichment in the ferroselite–trogtalite assemblage seems to be connected with the increase in Co (Fig. 3a), and not in Pb (Fig. 3b), making unlikely any significant contribution of Au from the ablation of matrix clausthalite. Indeed, Ramdohr and Schmitt (1955) observed native Au within an atoll-like microstructure of corroded trogtalite, which is analogous to Fig. 2. The corrosion of trogtalite likely liberated its trace amounts of Au, which locally precipitated as native Au within the atoll-like microstructure.

Because pyrite has extensively been analysed for minor and trace elements, in particular for Co, Ni and Au, the following discussion on the Trogtal ferroselite refers to pyrite. To our knowledge, trace-element data for ferroselite have not yet been reported in the literature.

Pyrite with $\text{Co/Ni} > 1$ has been used to distinguish pyrite of volcanogenic origin (e.g., Bralía et al. 1979; Marques et al. 2006), in particular where high-salinity brines interacted with volcanic host rocks. For example, Cl-rich fluids, which have $\text{Co/Ni} > 1$ (Douville et al. 2002), are thought to have formed volcanogenic pyrite that is also distinguished by $\text{Co/Ni} > 1$ (Marques et

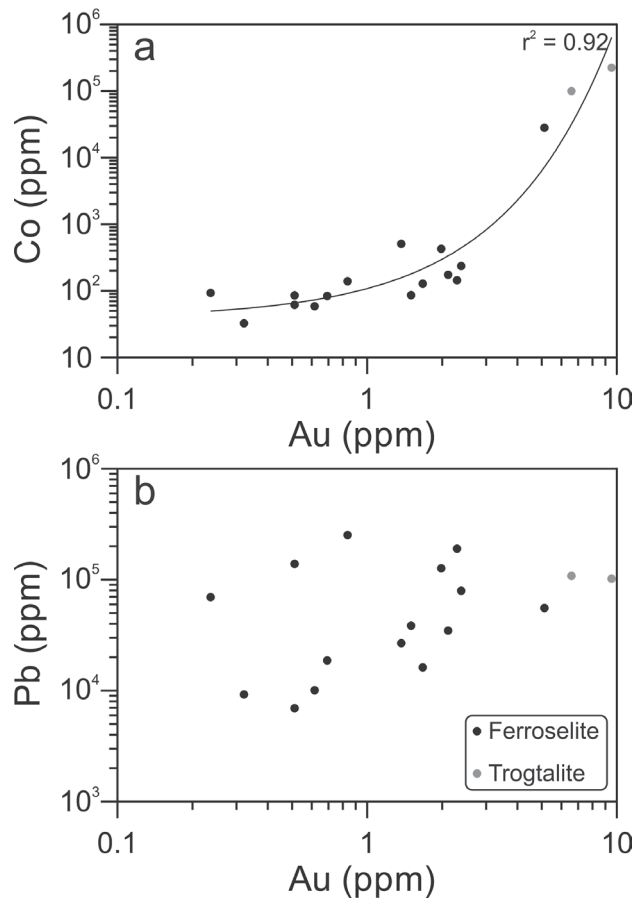


Fig. 3 Plots of Au vs. Co (a) and Au vs. Pb (b) from LA-ICP-MS analyses (Tab. 2). In a, the metals are positively correlated in an exponential fashion (squared correlation coefficient, r^2 , of 0.92); in b, the metals show a scattered distribution.

al. 2006). Similarly, Pal et al. (2011) have argued that the chemical composition of their hydrothermal pyrite, which is enriched in Co with $\text{Co/Ni} > 1$, fingerprints a high-salinity fluid. The assumption that fluids of high salinity are capable of fractionating Co from Ni finds support in the economically important concentrations of Co in the Zambian Copperbelt, the genesis of which has been explained by high-salinity sedimentary brines that transported metals in solution (e.g., McGowan et al. 2006; Koziy et al. 2009). Cobalt-bearing pyrite and Pd-containing trogtalite have been documented from African sediment-hosted Cu deposits (e.g., Craig and Vaughan 1979; Pirard and Hatert 2008).

The Au-bearing ferroselite and the evidence for some Pd and Pt in the associated trogtalite, together with the reddish greywacke, genetically link Trogtal to the hydrothermal milieu of sediment-hosted Cu deposits, in which precious metals are found spatially associated with oxidized rocks (e.g., Oszcsepalski 1999; Shepherd et al. 2005). This oxidation has been attributed to basinal brines (e.g., Jowett 1986; Kucha and Pawlikowski 1986; McGowan et al. 2006). Such brines led to metal

concentrations that typically have $\text{Co/Ni} > 1$, as reported for the Kupferschiefer at Sangerhausen, in the vicinity of the Harz (Hammer et al. 1990; Sun and Püttmann 1997). In the Kupferschiefer of Poland, epigenetic pyrite is also characterized by Co/Ni ratios above unity (Kucha and Pawlikowski 1986). The Trogtal ferroselite, predominantly of $\text{Co/Ni} > 1$, could thus be interpreted to have formed from oxidizing, Kupferschiefer-like brines. It is important to note here that the selenide vein-hosting Carboniferous greywacke was primarily overlain by the Zechstein evaporitic sequences (i.e., Late Permian; e.g., Ziegler 1978), which were eroded during rapid uplift of the Harz in Late Cretaceous times (e.g., von Eynatten et al. 2008). The Zechstein could explain the existence of such highly saline fluids.

Our interpretation for the ferroselite Co/Ni ratio, as a fingerprint of high-salinity brines of Kupferschiefer type, needs to be supported by fluid-inclusion data. Such data are not available for Trogtal, but for other metalliferous deposits in the Harz (e.g., Lüders and Möller 1992). They indicate that the vein deposits of the Harz formed in post-Variscan times from high-salinity brines at temperatures within the epithermal range. Based on its selenide–hematite assemblage, Trogtal can be regarded as belonging to the earliest stage of post-Variscan mineralization (e.g., Kuschka and Franzke 1974; see Tab. 1 of Lüders and Möller 1992). This temporal positioning of Trogtal would be consistent with the Late Permian age that Brauns et al. (2003) established for the Kupferschiefer mineralization at Sangerhausen – considering its syngenetic or early-diagenetic nature (e.g., Wedepohl and Rentzsch 2006). However, a new age proposed for the Kupferschiefer mineralization at Sangerhausen, Late Jurassic (Symons et al. 2011), favors an epigenetic model. Such a late timing could suggest that the hematitization and associated seleniferous veins at Trogtal might be temporally linked with the epigenetic Kupferschiefer mineralization. Hydrothermal overprint involving oxidizing fluids resulted in vein-type mineralization in Permo–Triassic sequences elsewhere in Europe (e.g., Dill 1988; Shepherd et al. 2005; Okrusch et al. 2007).

6. Conclusions

The ferroselite at Trogtal (Harz Mountains, Germany) contains trace amounts of Au, from 0.2 to 5.1 ppm, which increase with Co abundance. Greater Au concentrations, 6.6 and 9.5 ppm, occur in trogtalite. Most Co/Ni ratios of ferroselite are above unity. These ratios, together with the reddened host greywacke and the specular hematite–selenide veins, suggest a hydrothermal environment of saline and oxidizing brines with $\text{Co/Ni} > 1$. Such fluid

characteristics are similar to those involved in the formation of sediment-hosted Cu deposits.

Acknowledgements. Professor Bernd Lehmann kindly reviewed an early version of the manuscript. ARC acknowledges the DFG (Deutsche Forschungsgemeinschaft, project CA 737/1-1) for financing his stay at Technische Universität Clausthal. Lukáš Ackerman and an anonymous reviewer greatly improved the manuscript by thoughtful comments and suggestions. František Laufek and Vojtěch Janoušek are thanked for their diligent editorial handling.

References

- BENZAAZOUA M, MARION P, ROBAUT F, PINTO A (2007) Gold-bearing arsenopyrite and pyrite in refractory ores: analytical refinements and new understanding of gold mineralogy. *Mineral Mag* 71: 123–142
- BRALIA A, SABATINI G, TROJA F (1979) A reevaluation of the Co/Ni ratio in pyrite as geochemical tool in ore genesis problems. *Miner Depos* 14: 353–374
- BRAUNS CM, PATZOLD T, HAACK U (2003) A Re–Os study bearing on the age of the Kupferschiefer mineralization at Sangerhausen. Abstracts, XVth International Congress of Carboniferous and Permian Stratigraphy, Utrecht, pp 66
- CABRAL AR, KOGLIN N (2012) Hydrothermal fluid source constrained by Co/Ni ratios in coexisting arsenopyrite and tourmaline: the auriferous lode of Passagem, Quadrilátero Ferrífero of Minas Gerais, Brazil. *Mineral Petrol* 104: 137–145
- CLARK C, GRGURIC B, SCHMIDT MUMM A (2004) Genetic implications of pyrite chemistry from the Palaeoproterozoic Olary Domain and overlying Neoproterozoic Adelaidean sequences, northeastern South Australia. *Ore Geol Rev* 25: 237–257
- COOK NJ, CIOBANU CL, MAO J (2009) Textural control on gold distribution in As-free pyrite from the Dongping, Huangtuliang and Hougou gold deposits, North China Craton (Hebei Province, China). *Chem Geol* 264: 101–121
- CRAIG JR, VAUGHAN DJ (1979) Cobalt-bearing sulfide assemblages from the Shinkolobwe deposit, Katanga, Zaire. *Amer Miner* 64: 136–139
- DILL H (1988) Geologic setting and age relationship of fluorite–barite mineralization in southern Germany with special reference to the Late Paleozoic unconformity. *Miner Depos* 23: 16–23
- DOUVILLE E, CHARLOU JL, OELKERS EH, BIENVENU P, JOVE COLON CF, DONVAL JP, FOUQUET Y, PRIEUR D, APPRIOU P (2002) The Rainbow vent fluids (36°14'N, MAR): the influence of ultramafic rocks and phase separation on

- trace metal content in Mid-Atlantic Ridge hydrothermal fluids. *Chem Geol* 184: 37–48
- FIGGE K (1964) Das Karbon am Nordwestende des Harzes. *Geol Jb* 81: 771–808
- FREBOLD G (1927a) Beiträge zur Kenntnis der Erzlagerstätten des Harzes. II. Über einige Selenerze und ihre Paragenesen im Harz. *Cb Mineral Geol Paläont A*: 16–32
- FREBOLD G (1927b) Beiträge zur Kenntnis der Erzlagerstätten des Harzes. III. Über Berzelianit, Cu_2Se , and ein neues Vorkommen von „Selenkobaltblei“ im Harz. *Cb Mineral Geol Paläont A*: 196–199
- HAMMER J, JUNGE F, RÖSLER HJ, NIESE S, GLEISBERG B, STIEHL G (1990) Element and isotope geochemical investigations of the Kupferschiefer in the vicinity of “Rote Fäule”, indicating copper mineralization (Sangerhausen Basin, G.D.R.). *Chem Geol* 85: 345–360
- JOWETT EC (1986) Genesis of Kupferschiefer Cu–Ag deposits by convective flow of Rotliegende brines during Triassic rifting. *Econ Geol* 81: 1823–1837
- KEUTSCH FN, FÖRSTER H-J, STANLEY CJ, RHEDE D (2009) The discreditation of hastite, the orthorhombic dimorph of CoSe_2 , and observations on trogtalite, cubic CoSe_2 , from the type locality. *Canad Mineral* 47: 969–976
- KOGLIN N, FRIMMEL HE, MINTER WEL, BRÄTZ H (2010) Trace-element characteristics of different pyrite types in Mesoarchaeon to Palaeoproterozoic placer deposits. *Miner Depos* 45: 259–280
- KOZIY L, BULL S, LARGE R, SELLEY D (2009) Salt as a fluid driver, and basement as a metal source, for stratiform sediment-hosted copper deposits. *Geology* 37: 1107–1110
- KUCHA H, PAWLIKOWSKI M (1986) Two-brine model of the genesis of strata-bound Zechstein deposits (Kupferschiefer type), Poland. *Miner Depos* 21: 70–80
- KUSCHKA E, FRANZKE HJ (1974) Zur Kenntnis der Hydrothermalite des Harzes. *Z geol Wiss* 2: 1417–1436
- LOFTUS-HILLS G, SOLOMON M (1967) Cobalt, nickel and selenium in sulphides as indicators of ore genesis. *Miner Depos* 2: 228–242
- LÜDERS V, MÖLLER P (1992) Fluid evolution and ore deposition in the Harz Mountains (Germany). *Eur J Mineral* 4: 1053–1068
- MAJZLAN J, CHOVAN M, ANDRÁŠ P, NEWVILLE M, WIEDENBECK M (2010) The nanoparticulate nature of invisible gold in arsenopyrite from Pezinok (Slovakia). *Neu Jb Mineral, Abh* 187: 1–9
- MARQUES AFA, BARRIGA F, CHAVAGNAC V, FOUQUET Y (2006) Mineralogy, geochemistry, and Nd isotope composition of the Rainbow hydrothermal field, Mid-Atlantic Ridge. *Miner Depos* 41: 52–67
- MCGOWAN RR, ROBERTS S, BOYCE AJ (2006) Origin of the Nchanga copper–cobalt deposits of the Zambian Copperbelt. *Miner Depos* 40: 617–638
- OKRUSCH M, LORENZ JA, WEYER S (2007) The genesis of sulfide assemblages in the former Wilhelmine mine, Spessart, Bavaria, Germany. *Canad Mineral* 45: 723–750
- OSZCZEPALSKI S (1999) Origin of the Kupferschiefer polymetallic mineralization in Poland. *Miner Depos* 34: 599–613
- PAL DC, SARKAR S, MISHRA B, SARANGI AK (2011) Chemical and sulphur isotope compositions of pyrite in the Jaduguda U (–Cu–Fe) deposit, Singhbhum shear zone, eastern India: implications for sulphide mineralization. *J Earth Syst Sci* 120: 475–488
- PIRARD C, HATERT F (2008) The sulfides and selenides of the Musonoï mine, Kolwezi, Katanga, Democratic Republic of Congo. *Canad Mineral* 46: 219–231
- RAMDOHR P (1928) Klockmannit, ein neues natürliches Kupferselenid. *Cb Mineral Geol Paläont A*: 225–232
- RAMDOHR P, SCHMITT M (1955) Vier neue natürliche Kobaltselenide vom Steinbruch Trogtal bei Lautenthal im Harz. *Neu Jb Mineral, Mh*: 133–142
- SHEPHERD TJ, BOUCH JE, GUNN AG, MCKERVEY JA, NADEN J, SCRIVENER RC, STYLES MT, LARGE DE (2005) Permo–Triassic unconformity-related Au–Pd mineralisation, South Devon, UK: new insights and the European perspective. *Miner Depos* 40: 24–44
- SUN Y, PÜTTMANN W (1997) Metal accumulation during and after deposition of the Kupferschiefer from the Sangerhausen Basin, Germany. *Appl Geochem* 12: 577–592
- SYMONS DTA, KAWASAKI K, WALTHER S, BORG G (2011) Paleomagnetism of the Cu–Zn–Pb-bearing Kupferschiefer black shale (Upper Permian) at Sangerhausen, Germany. *Miner Depos* 46: 137–152
- TISCHENDORF G (1959) Zur Genesis einiger Selenidvorkommen, insbesondere von Tilkerode im Harz. *Freiberg Forsch H C* 69, pp 1–168
- THOMAS HV, LARGE RR, BULL SW, MASLENNIKOV V, BERRY RF, FRASER R, FROUD S, MOYE R (2011) Pyrite and pyrrhotite textures and composition in sediments, laminated quartz veins, and reefs at Bendigo gold mine, Australia: insights for ore genesis. *Econ Geol* 106: 1–31
- VAN ACHTERBERGH E, RYAN CG, GRIFFIN WL (2000) GLITTER (version 3.0, on-line interactive data reduction for LA-ICPMS). Macquarie Research Ltd.
- VON EYNATTEN H, VOIGT T, MEIER A, FRANZKE H-J, GAUPP R (2008) Provenance of Cretaceous clastics in the Subhercynian Basin: constraints to exhumation of the Harz Mountains and timing of inversion tectonics in Central Europe. *Int J Earth Sci (Geol Rundsch)* 97: 1315–1330
- WAGNER T, KLEMD R, WENZEL T, MATSSON B (2007) Gold upgrading in metamorphosed massive sulfide ore deposits: direct evidence from laser-ablation–inductively coupled plasma–mass spectrometry analysis of invisible gold. *Geology* 35: 775–778

WEDEPOHL KH, RENTZSCH J (2006) The composition of brines in the early diagenetic mineralization of the Permian Kupferschiefer in Germany. *Contrib Mineral Petrol* 152: 323–333

WOHLGEMUTH-UEBERWASSER CC, BALLHAUS C, BERNDT J, STOTTER NÉE PALIULIONYTE V, MEISEL T (2007) Synthesis

of PGE sulfide standards for laser ablation inductively coupled plasma mass spectrometry (LA-ICP-MS). *Contrib Mineral Petrol* 154: 607–617

ZIEGLER PA (1978) North-Western Europe: tectonics and basin development. *Geol Mijnb* 57: 589–626